Monitoring water stress using time series of observed to unstressed surface temperature difference

Gilles Boulet, Abdelghani Chehbouni, P. Gentine, Benoît Duchemin, J. Ezzahar, R. Hadria

Available online at www.sciencedirect.com
ScienceDirect
Agricultural and Forest Meteorology 146 (2007) 159–172
AGRICULTURAL AND FOREST METEOROLOGY
www.elsevier.com/locate/agrformet

Monitoring water stress using time series of observed to unstressed surface temperature difference

G. Boulet [a,*], A. Chehbouni [a], P. Gentine [c], B. Duchemin [a], J. Ezzahar [b], R. Hadria [b]

[a] *Centre d'Etudes Spatiales de la BIOsphère, Toulouse, France*
[b] *Université Cadi Ayyad, Marrakech, Morocco*
[c] *Department of Civil & Environmental Engineering, MIT, USA*

Received 19 July 2006; received in revised form 3 May 2007; accepted 25 May 2007

Abstract

Remote sensing data in the thermal infra red (TIR) part of the spectrum provides indirect estimates of water stress – defined as a function of the ratio between actual and potential evaporation rates – at the earth surface. During the first stage of evaporation (''energy limited'' evaporation), this ratio is close to one. During the second stage of evaporation (''soil controlled'' evaporation) water stress occurs and as a result this ratio drops below one. Recently, methods using TIR data to monitor stress have shifted from establishing empirical relationships between combined vegetation cover/temperature indices and soil moisture status to data assimilation of surface temperature into complex soil–vegetation–atmosphere transfer models. However, data and expertise are often lacking to widely apply those methods. In this paper we investigate the proof-of-concept of using solely the difference between actual and unstressed surface temperature as a baseline to monitor water stress. The unstressed temperature is the equilibrium temperature of a given surface expressed in potential conditions, computed with an energy balance model. Theoretical, modelling, and experimental documentation of the proof-of-concept are shown for datasets acquired within the frame of two international experiments in semi-arid region. We show that the difference between the observed and the unstressed surface temperatures is almost linearly related to water stress. A sensitivity study is carried out to test the impact of modelling errors on the evaluation of the unstressed temperature. We found that even with inaccurate but realistic values of the surface parameters used to solve the energy balance and compute the unstressed temperature, the observed to unstressed surface temperature difference is still more relevant to detect second-stage processes than the difference between the observed surface temperature and the air temperature. The perspective of using an empirical index based on this difference is also investigated. These results are especially attractive for application based on TIR satellite imagery at a regional scale.

Keywords: Water stress; SVAT model; Radiative surface temperature; Remote sensing; Semi arid

1. Introduction

Detection of crop water stress is crucial for efficient irrigation water management, especially in semi-arid regions. Water stress, or second-stage evaporation (Levine and Salvucci, 1999), corresponds to the reduction in evaporation due to the limited availability of root zone soil moisture. Water stress results in a drop of actual evaporation below the potential rate. Its intensity is usually represented by a Stress Factor (S), which is defined more generally by the complement to one of the actual (λE) to potential (λE_p) evaporation ratio:

$$S = 1 - \frac{\lambda E}{\lambda E_p} \quad (1)$$

* Corresponding author.
E-mail address: gilles.boulet@cesbio.cnes.fr (G. Boulet).

0168-1923/$ – see front matter © 2007 Elsevier B.V. All rights reserved.
doi:10.1016/j.agrformet.2007.05.012

This factor is equal to zero for energy-limited evaporation (unstressed conditions), and increases towards one for soil-controlled evaporation (water stress conditions).

Water stress can be assessed by measuring evaporation rates, and evaluate potential evaporation using classical methods such as Penman-Monteith or an energy balance model by setting the surface resistance to a minimal value. Measurements of total evaporation (λE) at the paddock scale can be achieved with the Eddy-covariance method, but this method is costly and needs well-trained staff to operate and maintain it. For larger scale (1 km and above) there is no observational device to measure routinely evaporation, except scintillometry. Scintillometers can provide estimates of the sensible heat flux for a cross-section of about 10 km (Kohsiek et al., 2002). λE can then be obtained as the residual term of the energy balance equation providing estimates of available energy at the same scale using remote sensing data (Ezzahar et al., 2007). These techniques are not trivial to set up and there is a large place to develop alternative methods for the monitoring of water stress.

Data in the thermal infra red (TIR) is linked to soil moisture and thus to the evaporation flux since the surface temperature is obtained through solving the surface energy balance equation. The use of TIR data to monitor stress can be classified into three broad categories (Courault et al., 2005). For each of these categories described below, TIR data can be combined or not to a surface energy balance model (see Table 1) in order to provide more elaborate information:

1. Using TIR data for an assessment of instantaneous flux patterns:

a. The first group of methods computes indices based on TIR radiance and a combination of surface reflectances: since index maps can be easily deduced from remote sensing images acquired in thermal and visible bands, these methods are very popular. Amongst such methods, one can mention the Crop Water Stress Index (CWSI: Jackson et al., 1981; Jackson, 1982), the Surface Energy Balance Index (SEBI: Menenti and Choudhury, 1993) or the Water Deficit Index (WDI: Moran et al., 1994; Moran, 2004); these indices are different expressions of the Stress Factor, and have been derived from a surface energy balance model. On the other hand, some indices like the Temperature–Vegetation Dryness Index (TVDI: Sandholt et al., 2002) or the Temperature Vegetation Index (TVI: Prihodko and Goward, 1997) do not rely on any parameterization of the energy balance and can be computed directly from remote-sensing data.

Stress indices are usually based on either the observed surface temperature itself or the difference between the observed surface temperature and air temperature at screen level (Sepulcre-Canto et al., 2006); they rely upon the assumption that for a given image there are places that evaporate at a potential rate ($S = 0$), and very dry, non-evaporating places ($S = 1$); stress levels are scaled according to the distance between the surface temperature of a given pixel and the minimum and maximum surface temperatures observed on the scene; these extreme values are related to the extreme values of S, i.e. 0 and 1; more recent studies also state that for each water stress condition the temperature depends on the amount of bare soil seen by the TIR sensor; the scaling between both extremes of S depends on a second remote-sensing variable representing the vegetation cover fraction, which is usually the Normalized Difference Vegetation Index (NDVI), or the Soil Adjusted Vegetation Index (SAVI); this leads to the classical triangle or trapezoidal shape of the temperature/vegetation cover diagram (Carlson et al., 1994; Moran et al., 1994; Boegh et al., 1999; Moran, 2004; Luquet et al., 2004) with its ‘‘cold’’ (unstressed) and ‘‘warm’’ (stressed) edges. The trapezoid method is often used to derive a spatial pattern of instantaneous stress level for a given TIR/NDVI image (Batra et al., 2006). Since the extreme vegetation and moisture conditions are not always present at the time of acquisition, it is not the most accurate way to represent the space/time variability of the hydric status. The use of time series of WDI

Table 1
Classification of some methods to assess water stress from TIR data.

	With an energy balance model	Without energy balance model
Instantaneous retrieval	SEBAL, ALARM, SEBS, etc.	TVI, TVDI, etc.
Time series analysis	CWSI, SEBI, WDI, etc.	Albedo, $T_s - T_a$, $(T_s - T_a)/R_s$, etc.
Data assimilation in a state-space model	Simple (thermal inertia only, no water balance involved) or complex (SVAT, water balance involved)	Assimilation of time to stress in water balance models (e.g. SVATsimple)

values computed with an energy balance model appears to be a better alternative to monitor water stress instead of mapping water stress levels.

b. The second family of methods involves a surface energy balance model: surface temperature is used as input to derive the sensible heat flux and obtain λE as a residual of the energy balance; flux maps are produced whenever an image is available. The first methods do not model explicitly the difference between the aerodynamic and the surface temperatures (Seguin and Itier, 1983; Lagouarde, 1991) whereas most recent methods parameterize this difference (Chehbouni et al., 1997) or provide an estimate of the kB^{-1} parameter (SEBAL: Bastiaanssen et al., 1998; SEBS: Su, 2002; ALARM: Suleiman and Crago, 2002). As for the indices mentioned above, some methods assume that on a given image there are places that evaporate at a maximum rate and other areas with no evaporation. To provide time series of λE, extrapolation methods like data assimilation are required to estimate fluxes for dates between two successive cloud-free images.

2. Using time series of TIR observations:

The second category of methods takes advantage of looking at TIR data time series. Amongst them, the first group, which does not involve any surface energy balance model, uses change detection algorithms and is based on the assumption that when the surface enters the ''soil controlled'' stage (this stage is also named ''supply-limited'' in some references), there are strong and sudden changes in surface conditions that impact on the surface temperature. For bare soil and short vegetation, Amano and Salvucci (1997) states that ''transitions from atmosphere-limited to soil-limited evaporation can be accompanied by either an increase in afternoon surface temperature relative to either air temperature or morning surface temperature, or an increase in land surface albedo''. The first advantage of using such methods is that they are catching the consistency between the evolution of TIR observations and the date of the last irrigation or rainfall event instead of computing instantaneous stress levels independently of the drying/wetting history. The other advantage is that systematic errors in observed surface temperature (constant bias) do not significantly affect the results of stress detection algorithms since the later are only looking at trends in the TIR data time series and not at absolute values. The second type of methods involves a surface energy balance model. Within this category, and amongst the most popular methods to use TIR data to monitor water stress, one can mention the analysis of time series of CWSI interpreted as the evolution in time of the Stress Factor (Jackson et al., 1981; Jackson, 1982). Finally, instantaneous indices can be compared for a limited number of dates with continuous time series of independent water status information: Sandholt et al. (2002) have found a good correlation between TVDI values and the soil moisture maps computed with a distributed hydrological model, whereas Goward et al. (2002) have found a good relationship between time series of TVI and surface soil moisture simulated by a complex soil vegetation atmosphere transfer (SVAT) model.

3. Assimilation of TIR data into land surface models:

Assimilation *sensu lato* enables to adjust either a state variable or a parameter of a given state-space process model in order to reduce the difference between the simulated and the observed radiometric surface temperatures. Whether the land surface model is based on the integration in time of the surface energy balance (in that case the only state variable is the soil temperature, taking into account the soil thermal inertia, e.g. Castelli et al., 1999) or the integration in time of the water balance (Boulet et al., 2002), or both (Demarty et al., 2004; Olioso et al., 2005), the problem is that model uncertainty, especially on the evaluation of soil thermal or hydrodynamical properties, is large. These methods, while interesting in the preparation of future observing systems (Pellenq and Boulet, 2004), have similar performances as more simple ones cited before (Jacob et al., 2006).

This study addresses possible improvements in the second category of methods, more specifically the use of time series of CWSI/WDI-type indices. The popular CWSI formulation proposed by Jackson et al. (1981) suffers from two major limitations: first, it does not take into account the temporal variability of the canopy structure and extent (Yuan et al., 2004); furthermore, it assumes that the surface and the aerodynamic temperatures are equal. Therefore, as stated by Moran (2004), ''Application of CWSI with satellite- or aircraft-based measurements of surface temperature is restricted to full-canopy conditions so that the surface temperature sensed is equal to canopy temperature''. Many other expressions of the Stress Factor are available in the literature. In the case of sparse vegetation or changing vegetation cover, Leaf Area Index can be used to modulate a single-source surface resistance (Moran et al., 1994) while Boegh et al. (2002) uses a decoupling coefficient to retrieve simultaneously an equivalent of

the surface resistance for the soil and for the canopy. In the ''trapezoid'' approach, Moran et al. (1994) show that the Stress Factor can be expressed as a function of two temperature boundaries in the NDVI versus $T_s - T_a$ space, the unstressed or ''cold edge'' (T_{sp}) and stressed or ''warm edge'' (T_{s0}) temperatures. This expression is called the Water Deficit Index (WDI):

$$S \cong \frac{T_s - T_{sp}}{T_{s0} - T_{sp}} \quad (2)$$

In (2), T_{s0} is the theoretical temperature of a non-evaporating surface with the same biophysical properties and climate conditions as the actual. It is calculated by solving the surface energy balance in actual conditions but replacing λE by 0. Computation of T_{s0} is not trivial, because it corresponds generally to high soil heat flux values (the soil thermohydric properties are not easy to evaluate at the appropriate space–time scale) as well as unstable convective conditions (which rely on semi-empirical stability functions). Similarly, heat exchange between the canopy and the soil for sparse conditions is not easy to evaluate when the soil is hot and dry but the plant is extracting water from the deep soil at a near-potential rate. In practice, model uncertainties in the evaluation of T_{sp} and T_{s0}, as well as measurement errors on T_s, can lead to erroneous CWSI/WDI estimates. Values of CWSI outside the range [0, 1] are not uncommon (Alderfasi and Nielsen, 2001; Barbosa da Silva and Ramana, 2005), especially in semi-arid regions where T_{s0} can reach very high values. Outside of the [0, 1] range, CWSI values cannot be interpreted as S estimates, and need to be rescaled accordingly. A practical solution to account for this discrepancy is to stretch the cold and warm edges simulated by a SVAT model to the boundaries of the observed trapezoid (Gillies et al., 1995). However, the use of the WDI is dependant on how one matches the ''observed'' trapezoid that is not always sampling all vegetation, moisture and atmospheric conditions and the ''simulated'' trapezoid computed with an energy balance model that should be adapted to those varying vegetation, moisture and atmospheric conditions. Furthermore, the retrieved stress level depends largely on the instantaneous shading conditions.

Acknowledging the limitations of the CWSI/WDI methods, many recent research avenues on stress detection have gone back to the interpretation of time series of surface to air temperature difference (Amano and Salvucci, 1997), or shifted to data assimilation. However, when data or expertise is lacking to apply SVAT models, the CWSI or WDI concept may be useful if it can be improved with the help of the recent progresses in the description of the surface energy balance components of SVAT models to provide simple yet robust stress indices derived from TIR data (Vidal and Devaux-Ros, 1995). In this study, instead of deriving a non-dimensional index, we propose to focus solely on the WDI numerator, i.e. the difference between the observed temperature and the temperature in potential conditions ($T_s - T_{sp}$).

The aim of this paper is two-fold: first, to document the theoretical, experimental and modelling evidences that the difference between the observed temperature and the temperature in potential conditions simulated with little *a priori* information on the land surface is a suitable information to monitor water stress under variable vegetation cover conditions, compared to ''classical'' indices based on observed variables alone (air to surface temperature difference, albedo, etc.); second, to assess the impact of model uncertainties on the accuracy of stress detection when a simple uncalibrated ''big leaf'' model is used to estimate the surface temperature in potential conditions, and rate this performance on a validation dataset for several vegetation types and conditions.

The paper is organized as follows: first the simple ''big leaf'' energy balance equation is run together with first guess parameter values to produce unstressed surface temperature and potential latent heat flux time series for three water stress periods identified within two experimental datasets. The evolution of both $T_s - T_a$ and $T_s - T_{sp}$ is then plotted against the observed and the potential latent heat fluxes to investigate the ability of both thermal indices to detect stress. Then the relationships between either $T_s - T_a$ or $T_s - T_{sp}$ and the Stress Factor S are identified by linearizing the ''big leaf'' model. In order to assess the variability of the linear regression coefficients, a physically-based ''reference'' SVAT model is applied for a wide range of vegetation and soil moisture conditions, first in known conditions, then when uncertainty in the energy balance components is synthetically taken into account. After this sensitivity analysis, the validity of the average linear relationship between $T_s - T_{sp}$ and S is checked against experimental data. Finally, some examples of application of this relationship are provided in conclusion.

1.1. Relevance of the $T_s - T_{sp}$ time series in monitoring stress

Coupling of the energy and the water exchange at the earth surface is only active when the atmospheric

conditions are not limiting the evaporation process; therefore under most circumstances there is no coupling and actual and potential conditions are identical. While the concept of potential evaporation is widely used in the literature (see Lhomme, 1997, for a review and a discussion of its definition), the concept of "temperature in potential conditions" is rarely used outside complex non-dimensional indices such as the WDI. The difference between the observed and the unstressed surface temperature is, in theory, sufficient to detect stress, but, since T_{sp} is the output of an energy balance model and is therefore prone to model and data errors, its proof-of-concept needs to be investigated. The foreseen advantage of concentrating on this difference is that detecting changes in $T_s - T_{sp}$ time series is easier than for the CWSI/WDI, since both uncertainty sources can be graphically represented: while model errors in the T_{sp} estimate can be deduced from specified parameter uncertainty, TIR observation errors can be deduced from remote sensing radiative transfer studies, independently of T_{s0} uncertainties, and also graphically displayed.

1.1.1. Experimental evidence: analysis of three water stress events

In this study, two datasets were used: the first one was collected during the SudMed project (Chehbouni et al., 2006) in 2003 over two patches of wheat whose size (4 ha) exceeds the basic fetch requirements: the B123 site under bare soil conditions and at a maximum Leaf Area Index L of 3, and the B27 site with a maximum L of 4; the second one was acquired during the SALSA experiment in 1997 (Goodrich et al., 2000) over a large sparse grassland field at two phenological stages: one at maximum development with a L of the order of 0.8 and the second at senescence with a starting L of 0.5. In both datasets, latent heat flux was measured with a Krypton (B27), a LICOR7500 (B123) or an EDISOL (SALSA) Fast Response Hygrometer and a 3D Sonic Anemometer with an embedded fast-thermocouple. TIR data was acquired with Everest Infra Red Thermometers (IRTs) looking at nadir with a 60° field of view at a height of 2.3 m (SALSA) and 2 m (SudMed). All IRTs have been calibrated using an Everest black body during the experiment and prior to the experiment in a laboratory with an adjustable ambient temperature. Other measurements include *in situ* classical meteorological forcing, albedo and Leaf Area Index. Experimental set-ups are presented in Boulet et al. (2000) for SALSA and Duchemin et al. (2006) (see also Er-Raki et al., 2007) for SudMed. For each site, stress was assessed by looking at time series of daily averaged observed latent heat flux (λE) and simulated latent heat flux in potential conditions (λE_p) during dry down periods in between two successive irrigations or rainfall events. λE_p was computed by solving the simple "big leaf" energy balance equation presented in Appendix A for the unstressed surface temperature (T_{sp}). Parameter values were taken from the middle of the *a priori* ranges given in Table 2, which can be considered as "realistic" average values for most continental surfaces. In order to match λE just after an irrigation (SudMed) or a major rainfall event (SALSA), λE_p was multiplied by an adjustment factor (from 0.9 for B27 to 1.1 for B123). This allows for compensating for measurement errors in λE or inaccurate parameter specification in simulated λE_p. Sharp divergence of λE from adjusted λE_p time series was interpreted as the starting date of water stress, or "time-to-stress". Two water stress periods were identified for B123 and SALSA, and one for B27 (see Figs. 1–3Figs. 1a-3a). It corresponds to 6-Mar. (B123 full cover, Fig. 1a), 27-Mar. (B27, Fig. 2a) and 4-Sep. (SALSA maximum cover, Fig. 3a). In parallel, time series of $T_s - T_a$ and $T_s - T_{sp}$ differences at midday were plotted for the

Table 2
Parameter range used in the random generation of actual (T_s,) and unstressed (T_{sp}) surface temperatures as well as actual (λE) and potential (λE_p) evaporation rates

Model	Parameter	Parameter range
Both models	Minimum stomatal resistance	20–200 (s m^{-1})
	Ratio of perturbated to observed Leaf Area Index (also applies for vegetation height)	0.5–1.5 (–)
"big leaf" model	Empirical parameter of the aerodynamic to surface temperature relationship	5–20 (–)
	Mixed surface albedo	0.15–0.3 (–)
ICARE-SVAT	Momentum to heat roughness lengths ratio	2–20 (–)
	Sand fraction	0–0.4 (–)
	Clay fraction	0–0.3 (–)
	Soil albedo	0.15–0.3 (–)
	Vegetation albedo	0.15–0.25 (–)
	Soil and vegetation emissivities	0.92–0.98 (–)

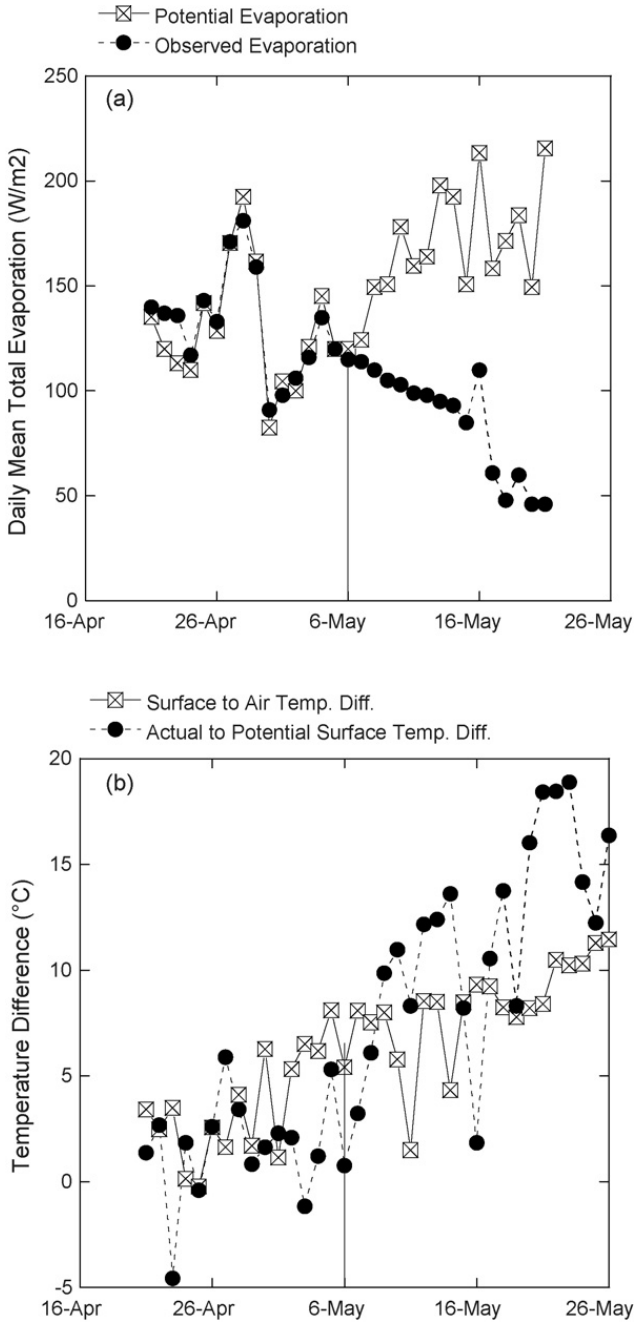

Fig. 1. Time series of daily averaged potential and observed total evaporation (a), and surface to air and potential to surface temperature difference at midday (b) in the case of the B123 wheat site at maximum development (full cover conditions). Vertical line designates the onset of water stress.

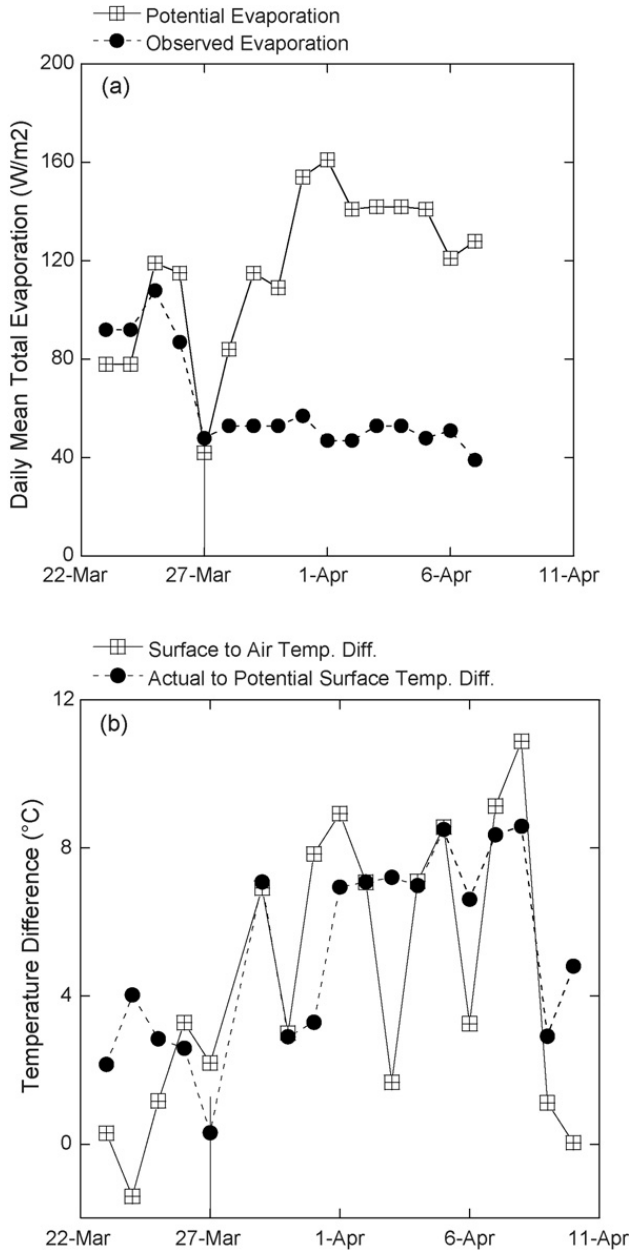

Fig. 2. Same as Fig. 1 for the B27 wheat site at maximum development (full cover conditions).

selected periods. For B123 and B27, both full cover (Figs. 1b and 2b) conditions show a quick increase in $T_s - T_{sp}$ after the time-to-stress but a continuous increase in $T_s - T_a$ before and after the time to stress. $T_s - T_{sp}$ is therefore a pertinent stress indicator in that case. In order to check that the increase in $T_s - T_{sp}$ is not due to senescence but rather to water stress before senescence, trends of other biophysical parameters, albedo and Leaf Area Index, are displayed on Fig. 4. Albedo values show a clear trend after senescence only, i.e. around 16-May, while water stress is present as early as 6-May. For the water stress period identified within the SALSA dataset (Fig. 3), it is not as clear as for SudMed. Both $T_s - T_{sp}$ and $T_s - T_a$ differences increase at the same time, two days after the time-to-stress.

1.1.2. Modelling evidence: linearization of the simple "big leaf" model

Surface temperature in potential conditions can be obtained through several parameterizations, the most

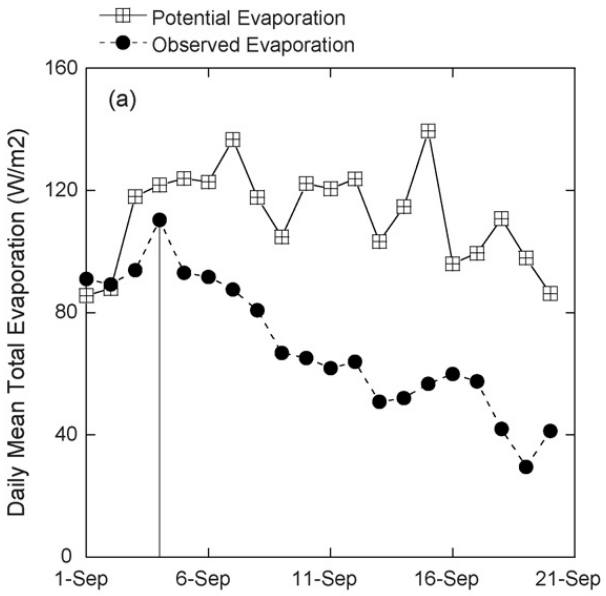

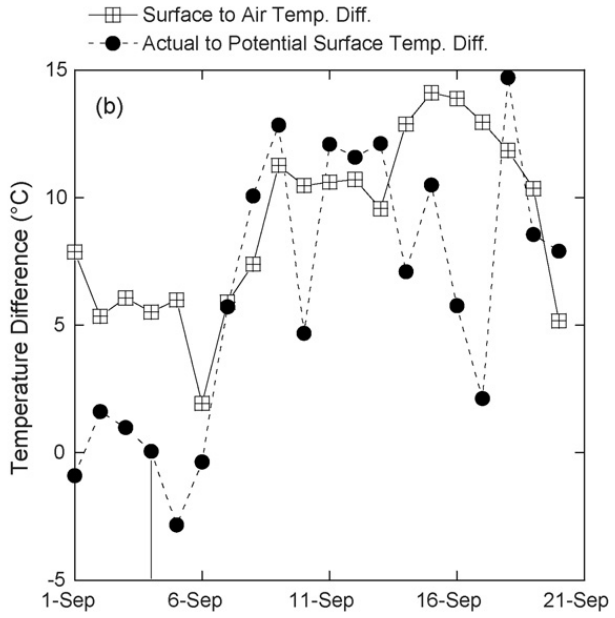

Fig. 3. Same as Fig. 1 in the case of the SALSA grassland site at maximum development.

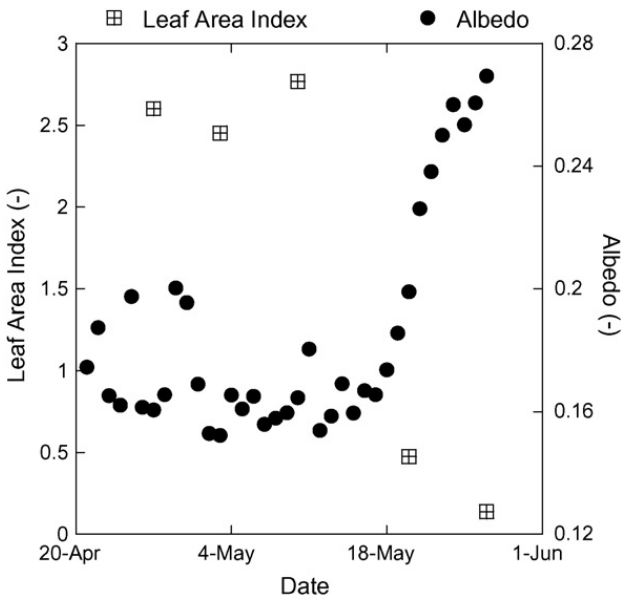

Fig. 4. Time series of Leaf Area Index and albedo for full cover conditions at the B123 wheat site.

simple being the Penman-Monteih equation (which is at the basis of the CWSI index), the most complex, yet computed in most SVAT models, being the simulated nadir radiometric temperature, which can be computed from different individual temperature components (for example the soil and the vegetation). In that case the soil and the vegetation surface temperatures can be derived by solving a dual-source (Shuttleworth and Wallace, 1985; Kustas and Norman, 1997) energy budget in potential conditions, and setting (1) the soil surface resistance and the stomatal resistance to a minimum value and (2) the soil heat flux to a fraction of the ground net radiation. In this section we will investigate the relationship between both $T_s - T_{sp}$ and $T_s - T_a$ temperature differences and S through the use of the simple "big leaf" energy balance equation. The complexity of this model lies between the Penman-Monteith and the dual-source energy balance expressions, and it can easily be linearized. It compensates for both limitations of the Penman-Monteith expression used in many studies (e.g. Moran et al., 1994; Vidal and Devaux-Ros, 1995): it takes into account the possible changes in vegetation cover conditions, and it relates the surface and the aerodynamic temperatures through an empirical function that depends solely on the Leaf Area Index (Chehbouni et al., 1997). The surface temperature T_{sp} and the aerodynamic temperature T_{0p} in potential conditions are obtained by solving the surface energy balance in potential conditions:

$$R_{np}(T_{sp}) = G_p(T_{sp}) + H_p(T_{0p}) + \lambda E_p(T_{0p}) \quad (3)$$

where R_n is the net radiation, G the ground heat flux, H the sensible heat flux and T_0 is the aerodynamic temperature, respectively. Subscript "p" stands for "computed in potential conditions".

The Stress Factor S can be written after linearization of (3) along T_a, as:

$$S = \frac{\lambda E_p - \lambda E}{\lambda E_p} = \frac{\varphi}{\lambda E_p}(T_s - T_{sp}) \quad (4)$$

where $\varphi = 4\varepsilon_s \sigma T_a^3 \zeta(1-\xi) + \rho c_p \zeta / r_{a0}$ (the definition of all symbols is provided in Appendix A).

Comparing stressed and unstressed conditions yields:

$$\lambda E_p = \varphi(T_{s0} - T_{sp}) \quad (5)$$

This means that the WDI expression (2) still holds for the "big leaf" formulation.

Since $T_{s0} - T_{sp} = \lambda E_p/\varphi$ is bounded and does not depend on S, there is a pseudo-linear relationship between $T_s - T_{sp}$ and S.

S can also be written as a linear combination of $T_s - T_a$:

$$S = \frac{\varphi}{\lambda E_p}(T_s - T_a) + \frac{\varphi}{\lambda E_p}(T_a - T_{sp}) \quad (6)$$

It is also a pseudo-linear relationship.

By looking at Eqs. (4) and (6), it becomes clear that a sharp increase in $T_s - T_{sp}$ and $T_s - T_a$ time series can only be interpreted as the starting point of water stress if (1) the dispersion of $T_s - T_{sp}$ and $T_s - T_a$ values around $S = 0$ is small, and (2) there is a clear and steady rise in temperature difference for low values of S. Comparing (4) and (6) shows that the linear regressions $T_s - T_{sp}$ versus S and $T_s - T_a$ versus S have the same apparent slope $1/(T_{s0} - T_{sp}) = \varphi/\lambda E_p$, but that $T_s - T_{sp}$ reacts more quickly to stress than $T_s - T_a$: for $T_s - T_a$, there is an offset in (6) around $S = 0$ which is proportional to the difference between T_{sp} and T_a. For temperate areas, this difference is generally small, but for semi-arid climates, as shown in the previous section, this difference can reach several degrees Celsius. In what follows, we use model simulation to analyse the variability of the slope $1/(T_{s0} - T_{sp}) = \varphi/\lambda E_p$ and the offsets of the linear regressions between S and either $T_s - T_{sp}$ or $T_s - T_a$.

1.1.3. Modelling evidence: generalization with a complex SVAT model

In order to check the sensitivity of the $T_s - T_{sp}$ versus S and $T_s - T_a$ versus S relationships for a wide range of soil moisture and vegetation conditions, we used a complex SVAT model as a reference or "benchmarking" tool to generate time series of T_s, T_{sp}, λE and λE_p. This synthetic dataset was simulated with the ICARE SVAT model (Gentine et al., 2007) for four months (February to May) of climate forcing at the B123 wheat crop site under actual and potential conditions (Fig. 5); this dataset is interesting because it spans a wide range of vegetation conditions (a full growing season with L values between 0 and 3) and soil moisture status (succession of wet conditions after irrigation or rainfall and long drying periods). ICARE is a physically-based soil–vegetation–atmosphere transfer model with a dual-source soil-plant interface and a multi-layer soil module. The energy balance is solved for two sources of radiation and turbulent heat fluxes, the soil and the vegetation. The water and the heat conduction in the soil are solved for soil moisture and temperature profiles using classical diffusion (heat) and convection-diffusion (water) equations (Richards, 1931). A moderate non-automatic calibration of the parameters was undertaken against observed time series of the energy budget (Rn, G, H, λE) and the water balance (soil moisture at different levels) in order to ensure the realism of the model's outputs (not shown). This simulation provides time series of a "reference" Stress Factor S (simulated) and the associated values of T_s and T_{sp} computed by running the model with the same input parameters for both actual and potential conditions. By plotting both temperature differences at 12AM against S, one can check that the correlation between $T_s - T_{sp}$ and S is much larger than the correlation between $T_s - T_a$ and S (Fig. 6). The pseudo-linear theoretical relationships (4) and (6) between S and $T_s - T_{sp}$ or $T_s - T_a$, respectively appear more clearly for $T_s - T_{sp}$. $T_s - T_{sp}$ shows a clear trend around $S = 0$, contrarily to $T_s - T_a$ which shows a large scatter of points corresponding to $\lambda E_p(T_{sp} - T_a)/\varphi$ values around $S = 0$ (Eq. (6)). It is quite interesting to see that the relationship between $T_s - T_{sp}$ and S is very linear, even though the conditions that prevail throughout the 2003 growing season vary drastically (bare soil, growing stage, maturity, senescence) over a large range of S values. This means that the slope $\theta = T_{s0} - T_{sp}$ of

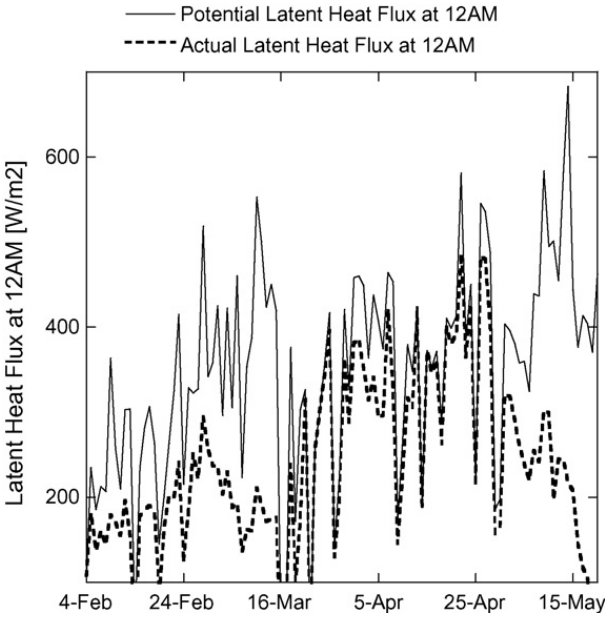

Fig. 5. Time series of instantaneous actual and potential latent heat flux values simulated with ICARE at midday for the B123 site dataset.

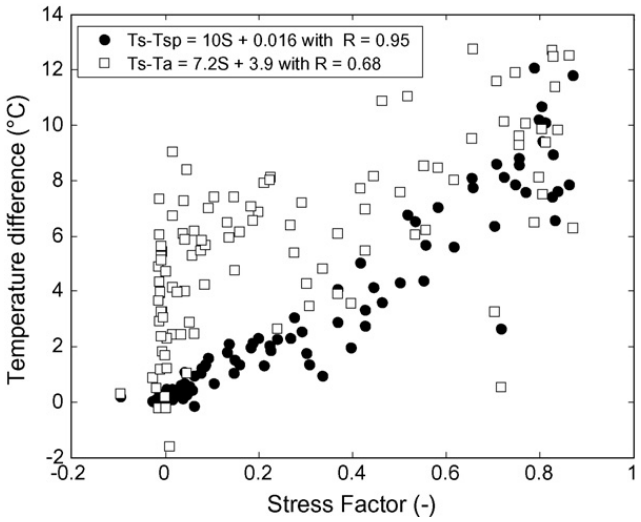

Fig. 6. Scatter plot of surface to air temperature difference ($T_s - T_a$) vs. Stress Factor (S) and actual to unstressed surface temperature difference ($T_s - T_{sp}$) vs. S simulated by ICARE at midday for the B123 site dataset.

the $T_s - T_{sp}$ versus S relationship is very stable across the different surface and atmospheric conditions, and could be represented by an average value for all vegetation, moisture and atmospheric conditions.

1.2. Impact of T_{sp} estimates uncertainty on index robustness

The different terms of S and $T_s - T_{sp}$ in the ''reference'' simulation presented above reflects the model's consistency in simulating stress. It does not account for uncertainty in $T_s - T_{sp}$ and $T_s - T_a$ estimates, and therefore for possible deviations from the pseudo-linear theoretical relationship due to simulation/model errors or instrumental biases. Errors associated with the evaluation of both TIR indicators falls within these two broad categories:

- measurement errors: georeferencing and registration shifts, sensor accuracy and spectral characteristics, atmospheric corrections, radiative transfer scheme inversion etc can all be responsible for errors in T_s estimates (see Jacob et al., 2006, for a review); spatial interpolation of the climate forcing, including T_a is also a source of error: meteorological forcing is usually taken from nearby climate stations which are not representative of the local climate and surface conditions; eventually, heterogeneity of the vegetation type and cover and other surface characteristics within the radiometric pixel or the instrumental field-of-view makes it difficult to interpret and fully understand the measurements.
- modeling errors: T_{sp} is derived from a model of the energy balance for a given surface. When one uses an energy balance model like the ''big leaf'' formulation, there are three parameters that are uncertain: (1) the minimum surface resistance to water vapour extraction, (2) the link between the aerodynamic and the surface temperature and (3) the ratio between the soil heat flux and the total net radiation. If a complex energy balance is used, for instance a dual-source expression (e.g. Braud et al., 1995) the most uncertain parameters are usually (1) the minimum stomatal resistance to water vapour extraction, (2) the parameters of the soil resistance to evaporation, and (3) the ratio between the soil heat flux and the total net radiation. Beyond the choice of the model, definition of ''potential conditions'' itself is not trivial. It is particularly true in the case of sparse vegetation, and, in general for intermediate values of L (growing stages for instance). Because the soil evaporation extracts water from the top soil whereas roots extract water on a larger soil depth, in most cases soil dries first, then the vegetation. Consequently, there are in fact three stages of evaporation for a given surface (Boulet et al., 2004). It is thus difficult to separate the decrease in soil evaporation rate from the vegetation water stress in a given time series of surface temperature. Possible confusion between both phenomena could be partly overcome by looking at directional temperatures (Boulet et al., 2001).

Given this large range of error sources, one could argue that although $T_s - T_a$ is related to stress with an unknown offset $\lambda E_p(T_{sp} - T_a)/\varphi$, $T_s - T_a$ does not depend on energy balance uncertainties (unlike T_{sp}), and might still be more relevant to monitoring water stress when T_{sp} is not known with precision. In order to check the performance of $T_s - T_{sp}$ over $T_s - T_a$ as a water stress indicator under uncertain conditions, a second synthetic analysis was performed. In this second analysis, in order to ensure a large uncertainty on T_{sp} estimates, T_{sp} was generated using a different model than ICARE, and many more ''reference'' cases than above were investigated. λE, λE_p and T_s were computed with ICARE under the same conditions as above, and instead of obtaining T_{sp} with ICARE, T_{sp} was calculated with the ''big leaf'' model presented in Appendix A with slightly different surface parameters than the ''reference'' simulation illustrated in Fig. 6. The ''big leaf'' model is a good compromise in terms of model complexity between the Penman-Monteith formulation and a dual-source energy balance, and sufficiently different from ICARE to provide a good benchmarking

estimate of T_{sp} errors. 100 "reference" simulations were produced by ICARE for surfaces randomly chosen according to their physical properties as a deviation to the simulation shown in Fig. 6; this was achieved by perturbing the most sensitive parameters using a randomly chosen set of parameters from a uniform distribution in the predefined intervals of variation (Table 2); then a surface temperature in potential conditions associated to each "reference" run was computed with a different randomly chosen set of parameters, using the very simple "big leaf" model presented in Appendix A (see also Table 2 for the range of parameters used to generate T_{sp} with the "big leaf" model); combining the "reference" λE and λE_p values simulated with ICARE provides a "reference" S. Combining the "reference" T_s and its associated T_{sp}, generated with the "big leaf" model, provides an estimate of $T_s - T_{sp}$ which can be compared to the "reference" difference $T_s - T_a$. The correlation coefficient of the linear regressions between both temperature differences and the Stress Factor was then computed for each of the 100 random simulations, i.e. the 100 "reference" combinations of λE, λE_p, T_s simulated with ICARE for 100 random sets of parameters and the 100 associated T_{sp} values simulated with the "big leaf" model for 100 other random sets of parameters. Fig. 7 shows the scatter plot of the correlation coefficient for one versus the other index (that is, the correlation coefficients of $T_s - T_a$ versus S and $T_s - T_{sp}$ versus S linear regressions). Even when there is a large uncertainty on modelled T_{sp}, $T_s - T_{sp}$ is still a more accurate indicator of stress than $T_s - T_a$. It is graphically evidenced on Fig. 7 by locating most (all except two) points under the [1:1] line. Linear regression coefficients are high enough to assume that even in uncertain conditions $T_s - T_{sp}$ can be used to monitor water stress.

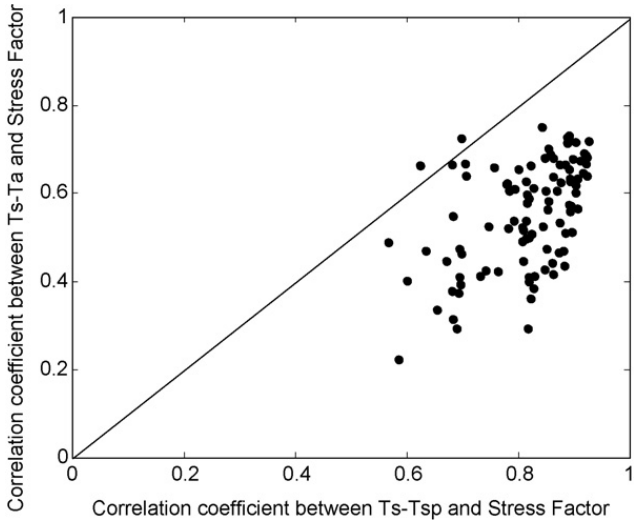

Fig. 7. Correlation coefficients of surface to air temperature difference ($T_s - T_a$) vs. Stress Factor (S) and actual to unstressed surface temperature difference ($T_s - T_{sp}$) vs. S linear regressions. T_s and S are simulated by ICARE while T_{sp} is simulated by the simple "big leaf" model for the B123 site dataset.

1.3. Identification, robustness and generality of the $S \cong (T_s - T_{sp})/\theta$ relationship

We have previously pointed out the need to look at time series of stress levels derived from TIR-based indicators to check their coherence with the irrigation and rainfall temporal patterns. For that purpose, we have shown in section A that isolating trends in $T_s - T_{sp}$ time series is relevant to stress detection. Moreover, it has been shown in the section B that $T_s - T_{sp}$ is almost always linearly related to S. It is therefore interesting to check if the empirical value of the slope of the pseudo-linear relationship obtained for the "reference" run ($S \cong (T_s - T_{sp})/10$, see Fig. 6) is robust and general enough to infer S instantaneously. This would provide a more simple index that could be used in place of a WDI. We must recall that according to (4) the denominator θ corresponds to the difference between the stressed and the unstressed theoretical temperatures ($T_{s0} - T_{sp}$) in given climatic conditions and for a given surface. Using an index of the form $(T_s - T_{sp})/\theta$ to infer the Stress Factor implies that θ is effectively stable for the whole range of S values. To do so, two conditions of the classical "split-sample" analysis are verified: (1) θ can be identified (i.e. it can be inferred for a given site during a calibration period), (2) its value must be robust (i.e. its performances in simulating stress for this site do not decrease in a validation period).

In order to check the existence of a quasi-constant $\theta = T_{s0} - T_{sp}$ value, the slope and offset of the linear regressions of $T_s - T_{sp}$ versus S for the 100 simulations presented in Fig. 7 were analysed; the mean and standard deviation for the offset are −0.15 and 0.14 °C, respectively, while for the slope it is 10.2 °C and 1.7 °C, respectively. These rather small standard deviations give us confidence in using $S \cong (T_s - T_{sp})/10$ as a rough but relevant estimate of S. In order to validate this relationship, a dataset collected during the growing season 2004 at the B124 field adjacent to B123, was used. λE_p and T_{sp} time series were calculated with the "big leaf" model presented in Appendix A, and the middle value of each parameter range as given in Table 2. It was combined with observed λE and T_s, respectively, to produce two estimates of S: the first is computed as $S = 1 - \lambda E/\lambda E_p$, the other is obtained from

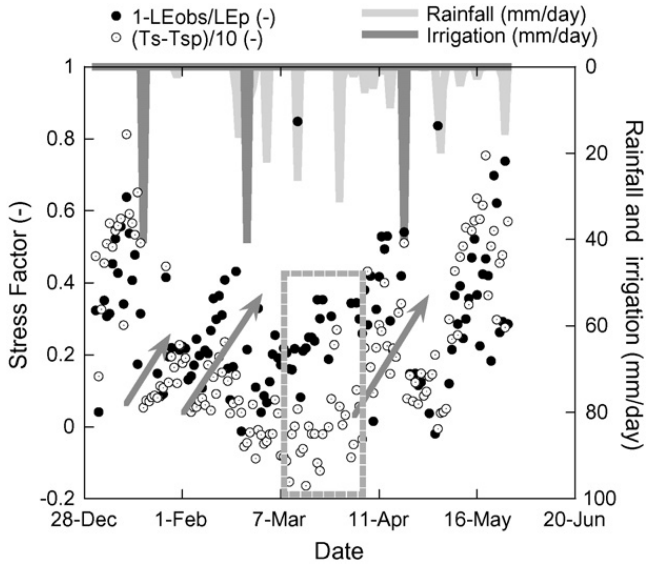

Fig. 8. Temporal evolutions of both estimates of Stress Factor for the B124 wheat site together with rainfall and irrigation: the observed Stress Factor $S = 1 - LE/LE_p$ (LE is the actual observed evaporation rate, LE_p is the potential evaporation rate computed with the simple "big leaf" model) and the empirical relationship $S \cong (T_s - T_{sp})/10$ (where T_s is the observed surface temperature measured by the thermoradiometer and T_{sp} the unstressed surface temperature computed with the simple "big leaf" model). The dashed rectangle shows the period for which the largest discrepancy between both estimates could be in favour of the empirical relationship: the low values around $S = 0$ are consistent with the number of rain events in that period.

the empirical relationship $S \cong (T_s - T_{sp})/10$. Note that the former cannot be seen as an exact "observed" S since λE_p was not adjusted to match observed λE after rainfall and irrigation (unlike Figs. 1–3) but evaluated using the average of the parameter range given in Table 2. Results are shown on Fig. 8 together with daily amounts of irrigation and rainfall. 2004 is a much wetter year than 2003, with little stress, and L peaks at about 4.2 around 1-April, while bare soil conditions prevail at the beginning (1–30 January) of the observation period. Vegetation is senescent at the end (10–30 May) of this period. S in bare soil and senescence conditions was well reproduced, while water status of some phenological stages, namely the growing and the end of maturity were less well reproduced (dotted grey box of Fig. 8). Several periods of increase in $S = 1 - \lambda E/\lambda E_p$ can be detected for periods of no-rain or no-irrigation (grey arrows of Fig. 8); they correspond roughly to an increase in $S \cong (T_s - T_{sp})/10$ with similar slopes, but a bias appears during early growth. $S = 1 - \lambda E/\lambda E_p$ is possibly overestimated for that stage given the number of rainfall events between 20-Feburay and 10-April This can be due to either an underestimation of λE (as indicated by the poor energy balance closure observed at that time) or an overestimation of λE_p. Note that $T_s - T_{sp}$ is always slightly positive, which means that measurement (T_s) and model (T_{sp}) errors are either small or compensate each other. It is an encouraging result, which would allow us to monitor water status over wheat in that region using thermal images cross-calibrated with our network of *in situ* IRTs.

Eventually, one could assume that the $S \cong (T_s - T_{sp})/\theta$ index could be used for many other herbaceous types of vegetation than wheat. In order to extrapolate this index to other surface types, data corresponding to Figs. 1–3 as well as two other similar events mentioned earlier (B123 bare soil and SALSA senescent vegetation) have been gathered into a single data frame to produce a scatter of points in the $T_s - T_{sp}$ versus S space. This dataset spans a wide range of surface types and vegetation water status. The determination coefficient of the S versus $T_s - T_{sp}$ linear regression is 0.57; its slope is 12.9 °C which is higher than the average value found for our wheat site and at the upper edge of the range of values obtained in the 100 simulations; moreover, there is an offset of 2.3 °C. The generality of an average θ value is thus questionable, and this last exercise should be carried out with more data.

2. Conclusion

Data in the thermal infra red spectrum is still nowadays the most promising data source to monitor water stress at most scales ranging from the paddock to the region. The Crop Water Stress Index proposed by Jackson et al. (1981) expresses the Stress Factor S with TIR data but is not valid for all surface conditions because of its simplifications on the energy balance. More recent methods to study water stress with the help of TIR data have shifted away from the S concept to more complex instantaneous diagrams based on surface cover or complex mathematical methods such as data assimilation. However, the unstressed limit of latent heat flux identified by an unstressed temperature can help the modeller as much as the experimentalist to detect and monitor water stress. For the modeller, there are two potential applications of this study:

1. T_{sp} should be equal to T_s just after a major rainfall event or large irrigation; adjusting the most sensitive parameters of the soil–vegetation–atmosphere interface (i.e. the system of equations of the surface energy balance) in order to reduce the $T_s - T_{sp}$ difference during the first stage of evaporation could lead to an evaluation of several parameters of the energy budget, including the minimum resistances, or the ratio

between the roughness lengths for momentum and sensible heat, or testing whether in unstressed conditions the atmosphere is always near-neutral; this should allow us to get rid of biases in this period more efficiently than assimilating T_s at any time.

2. Since $T_s - T_{sp}$ increases sharply when the surface enters the second stage of evaporation, trend analysis can be used to assess the starting point of this second stage. Time-to-stress depends on water diffusion in the soil; knowledge of the time-to-stress can thus be used to assess the soil hydrodynamic properties, or the equivalent parameterization of stress in more conceptual models. In models like SVATsimple (Boulet et al., 1999), time-to-stress is analytically related to the hydrodynamical parameters, the initial water content and λE_p. Hydrodynamical parameters can thus be analytically inverted from time-to-stress, initial water content and λE_p estimates, which saves complex calibration procedures in a data assimilation prospective (Demarty et al., 2004): if λE_p is correct, then one can concentrate on hydrodynamical parameter estimation during the second stage of evaporation, contrarily to classical "automatic" assimilation schemes, which use T_s directly as an input at all time.

For the experimentalist, the generality of simple empirical indices of the form $S \cong (T_s - T_{sp})/\theta$ is a promising research avenue. Simple models such as the one presented here could be used to derive T_{sp}. It could be interesting as well to test its performance for a wider range of vegetation types, such as clumped grass, or small shrubs, and to very heterogeneous terrains, prior to its application at larger scales.

Finally, this proof-of-concept is supporting the interest for satellite mission proposals such as IRSUTE (Seguin et al., 1999) that would provide estimates of the surface temperature with a typical daily revisit period. Indeed, with current satellite revisit capabilities at the ~100 m pixel resolution (a resolution compatible with most agronomical applications), successive acquisitions of TIR images are interspaced with large periods of time (~15 days) which can include several rainfall events. Some satellites offer a higher revisit frequency, but for a much coarser resolution (of the order of 1 km) often incompatible with the scale of application. Therefore, using radiation fluxes, albedo, emissivity, and LAI values deduced from the existing frequent (every 2–3 days) high and low resolution Remote-Sensing data would help to derive maps of unstressed temperatures only if it could be combined with series of observed surface temperature images from a high-resolution IRT sensor such as IRSUTE. Then, estimates of pixel-to-pixel water stress levels could be derived with the proposed method once a proper θ value is specified.

Acknowledgements

Support from PNTS (French "Programme National de Télédétection Spatiale") and INCO-MED European Program IRRIMED ('Improved management tools for water-limited irrigation: combining ground and satellite information through models', see http://www.irrimed.org) are gratefully acknowledged. Additional funding was provided through EU Pleiades project. Data for the B27 field site was collected by Dr. A. Olioso from INRA, and the authors want to thank him for his help and for the fruitful scientific discussions at the early stages of this work. The authors wish to thank Julio Rodriguez and Chris Watts from IMADES, Mexico, for their help in collecting the SALSA dataset. Both anonymous reviewers are also thanked for their useful contributions to improve the paper.

Appendix A

The Simple "big leaf" energy balance model (Boulet et al., 2000).

T_{sp} is the solution of the following energy balance equation:

$$[(1-a_s)R_s + \sigma\varepsilon_s(\varepsilon_a T_a^4 - T_{sp}^4)](1-\xi(L)) = \rho c_p \zeta\left(\frac{T_{sp}-T_a}{r_a(T_{sp})}\right) + \frac{\rho c_p}{\gamma}\left(\frac{e^*[T_0(T_{sp})]-e_a}{r_a(T_{sp})+r_s(L)}\right)$$

where ρ is the air density, c_p is the specific heat of air at constant pressure, a_s is the surface albedo, R_s the incoming solar radiation, ε_s the surface emissivity, ε_a the air emissivity, σ the Stefan–Boltzman constant, T_a the air temperature, soil heat flux G is a fraction $\xi(L)$ of the net radiation R_n depending on the Leaf Area Index (L), T_0 is the aerodynamic temperature, $\zeta = (T_{0p} - T_a)/(T_{sp} - T_a) = (e-1)/(e^{\upsilon/(\upsilon-L)} - 1)$ relates T_0 to the surface temperature T_{sp} according to L and an empirical parameter υ (Chehbouni et al., 1997), $r_a = r_{a0}(1/(1 + Ri(T_{0p} - T_a)))^{\eta}$ is the aerodynamic resistance relating the aerodynamic resistance without stability correction r_{a0} to the Richardson number Ri which is a function of the $T_{sp} - T_a$ difference, $\eta = 0.75$ in unstable conditions and $\eta = 2$ in stable conditions, e^* is the saturation vapour pressure at a given temperature, e_a is the current air vapour pressure,

$$r_s(L) = \begin{cases} r_{c_{min}} L & \text{if } L < 1 \\ r_{c_{min}}/L & \text{if } L \geq 1 \end{cases}$$

is the surface resistance and $r_{c_{min}}$ the minimum stomatal resistance.

One can note that with the above notations $\lambda E_p = \frac{\rho c_p}{\gamma}((e^*(T_0(T_{sp})) - e_a)/(r_a(T_{sp}) + r_s(L)))$

References

Alderfasi, A.A., Nielsen, D.C., 2001. Use of crop water stress index for monitoring water status and scheduling irrigation in wheat. Agric. Water Manage. 47 (1), 69–75.

Amano, E., Salvucci, G.D., 1997. Detection of three signatures of soil-limited evaporation. Remote Sens. Environ. 67 (1), 108–122.

Barbosa da Silva, B.T.V., Ramana, Rao, 2005. The CWSI variations of a cotton crop in a semi-arid region of Northeast Brazil. J. Arid Environ. 62 (4), 649–659.

Bastiaanssen, W.G.M., Menenti, M., Feddes, R.A., Holtslag, A.A.M., 1998. A remote sensing surface energy balance algorithm for land (SEBAL). 1. Formulation. J. Hydrol. 212–213, 198–212.

Batra, N., Islam, S., Venturini, V., Bisht, G., Jiang, L., 2006. Estimation and comparison of evapotranspiration from MODIS and AVHRR sensors for clear sky days over the Southern Great Plains. Remote Sens. Environ. 103 (1), 1–15.

Boegh, E., Soegaard, H., Hanan, N., Kabat, P., Lesch, L., 1999. A remote sensing study of the NDVI-Ts relationship and the transpiration from sparse vegetation in the Sahel based on high-resolution satellite data. Remote Sens. Environ. 69 (3), 224–240.

Boegh, E., Soegaard, H., Thomsen, A., 2002. Evaluating evapotranspiration rates and surface conditions using Landsat TM to estimate atmospheric resistance and surface resistance. Remote Sens. Environ. 79 (2–3), 329–343.

Boulet, G., Chehbouni, A., Braud, I., Duchemin, B., Lakhal, A., 2004. Evaluation of a two-stage evaporation approximation for contrasting vegetation cover. Water Resour. Res. 40, W12507, doi:10.1029/2004WR003212.

Boulet, G., Chehbouni, A., Braud, I., Vauclin, M., 1999. Mosaic versus dual source approaches for modeling the surface energy balance of a semi-arid land. J. Hydrol. Earth Sys. Sci. 3 (2), 247–258.

Boulet, G., Chehbouni, A., Braud, I., Vauclin, M., Haverkamp, R., Zammit, C., 2000. A simple water and energy balance model designed for spatialisation and remote sensing data utilization. Agric. Forest Meteorol. 105, 117–132.

Boulet, G., Chehbouni, A., Magnac, M., Kerr, Y., 2001. Time course of dual angle temperatures: implication for hydraulic properties evaluation. In: IGARSS'01, Sydney, Australia.

Boulet, G., Kalma, J.D., Kerr, Y.H., Chehbouni, A., 2002. Deriving catchment-scale water and energy balance parameters using data assimilation based on Extended Kalman Filtering. Hydrol. Sci. J. 47 (3), 449–467.

Braud, I., Dantas-Antonino, A.C., Vauclin, M., Thony, J.L., Ruelle, P., 1995. A simple soil–plant–atmosphere transfer model (SiSPAT), development and field verification. J. Hydrol. 166, 231–260.

Carlson, T.N., Gillies, R.R., Perry, E.M., 1994. A method to make use of thermal infrared temperature and NDVI measurements to infer surface soil water content and fractional vegetation cover. Remote Sens. Rev. 9, 161–173.

Castelli, F., Entekhabi, D., Caporali, E., 1999. Estimation of surface heat flux and an index of soil moisture using adjoint-state energy balance. Water Resour. Res. 35 (10), 3115–3125.

Chehbouni, A., Lo Seen, D., Njoku, E.G., Lhomme, J.-P., Monteny, B., Kerr, Y., 1997. Estimation of sensible heat flux over sparsely vegetated surfaces. J. Hydrol. 188–189, 855–868.

Chehbouni, A., Escadafal, R., Boulet, G., Duchemin, B., Simonneaux, V., Dedieu, G., Mougenot, B., Khabba, S., Kharrou, H., Merlin, O., Chaponniere, A., Ezzahar, J., Er-Raki, S., Hoedjes, J., Hadria, R., Abourida, H., Cheggour, A., Raibi, F., Hanich, L., Guemouria, N., Chehbouni, Ah., Olioso, A., Jacob, F. and Sobrino, J., 2006. The use of remotely sensed data for integrated hydrological modeling in arid and semi-arid regions: the SUDMED program, in press.

Courault, D., Seguin, B., Olioso, A., 2005. Review on estimation of evapotranspiration from remote sensing data: from empirical to numerical modeling approaches. Irrig. Drainage Syst. 19, 223–249.

Demarty, J., Ottlé, C., Braud, I., Olioso, A., Frangi, J.P., Bastidas, L., Gupta, H.V., 2004. Using a multiobjective approach to retrieve information on surface properties used in a SVAT model. J. Hydrol. 287, 214–236.

Duchemin, B., Hadria, R., Erraki, S., Boulet, G., Maisongrande, P., Chehbouni, A., Escadafal, R., Ezzahar, J., Hoedjes, J.C.B., Kharrou, M.H., 2006. Monitoring wheat phenology and irrigation in Central Morocco: on the use of relationships between evapotranspiration, crops coefficients, leaf area index and remotely-sensed vegetation indices. Agric. Water Manage. 79 (1), 1–27.

Er-Raki, S., Chehbouni, A., Guemouria, N., Duchemin, B., Ezzahar, J., Hadria, R., 2007. Combining FAO-56 model and ground-based remote sensing to estimate water consumptions of wheat crops in a semi-arid region. Agric. Water Manage. 87, 41–54.

Ezzahar, J., Chehbouni, A., Hoedjes, J.C.B., Chehbouni, Ah, 2007. On the application of scintillometry over heterogeneous surfaces. J. Hydrol. 334, 493–501.

Gentine, P., Entekhabi, D., Chehbouni, G., Boulet, G., Duchemin, B., 2007. Analysis of evaporative fraction diurnal behavior. Agric. Forest Meteorol. 143, 13–29.

Gillies, R.R., Carlson, T.N., Cui, J., Kustas, W.P., Humes, K.S., 1995. A verification of the 'triangle' method for obtaining surface soil water content and energy fluxes from remote measurements of the Normalized Difference Index (NDVI) and surface radiant temperature. Int. J. Remote Sens. 18 (15), 3145–3166.

Goodrich, D.C., Chehbouni, A., Goff, B., MacNish, B., Maddock, T., Moran, S., Shuttleworth, W.J., Williams, D.G., Watts, C., Hipps, L.H., Cooper, D.I., Schieldge, J., Kerr, Y.H., Arias, H., Kirkland, M., Carlos, R., Cayrol, P., Kepner, W., Jones, B., Avissar, R., Begue, A., Bonnefond, J.-M., Boulet, G., Branan, B., Brunel, J.P., Chen, L.C., Clarke, T., Davis, M.R., DeBruin, H., Dedieu, G., Elguero, E., Eichinger, W.E., Everitt, J., Garatuza-Payan, J., Gempko, V.L., Gupta, H., Harlow, C., Hartogensis, O., Helfert, M., Holifield, C., Hymer, D., Kahle, A., Keefer, T., Krishnamoorthy, S., Lhomme, J.-P., Lagouarde, J.-P., Lo Seen, D., Luquet, D., Marsett, R., Monteny, B., Ni, W., Nouvellon, Y., Pinker, R., Peters, C., Pool, D., Qi, J., Rambal, S., Rodriguez, J., Santiago, F., Sano, E., Schaeffer, S.M., Schulte, M., Scott, R., Shao, X., Snyder, K.A., Sorooshian, S., Unkrich, C.L., Whitaker, M., Yucel, I., 2000. Preface paper to the Semi-Arid land–surface–atmosphere (SALSA) program special issue. Agric. Forest Meterorol. 105 (1–3), 3–20.

Goward, S.N., Xue, Y., Czajkowski, K.P., 2002. Evaluating land surface moisture conditions from the remotely sensed temperature/vegetation index measurements: An exploration with the simplified simple biosphere model. Remote Sens. Environ. 79 (2–3), 225–242.

Jackson, R.D., 1982. Canopy temperature and crop water stress. Adv. Irrigation 1, 43–85.

Jackson, R.D., Reginato, R.J., Idso, S.B., 1981. Canopy temperature as a crop water stress indicator. Water Resour. Res. 17, 1133–1138.

Jacob, F., Schmugge, T., French, A., Ogawa, K., Olioso, A., Petitcolin, F., Chehbouni, G., Pinheiro, A., Privette, J., 2006. Modeling and inversion in thermal infrared remote sensing over vegetated land surfaces. In: Advances in Land Remote Sensing: System, Modeling, Inversion and Application, Springer.

Kohsiek, W., Meijninger, W.M.L., Moene, A.F., Heusinkveld, B.G., Hartogensis, O.K., Hillen, W.C.A.M., De Bruin, H.A.R., 2002. An extra large aperture scintillometer for long range applications. Bound. Layer Meteorol. 105, 119–127.

Kustas, W.P., Norman, J.M., 1997. A two-source approach for estimating turbulent fluxes using multiple angle thermal infrared observations. Water Resour. Res. 33 (6), 1495–1508.

Lagouarde, J.-P., 1991. Use of NOAA AVHRR data combined with an agrometeorological model for evaporation mapping. Int. J. Remote Sens. 12 (9), 1853–1864.

Levine, J.B., Salvucci, G.D., 1999. Characteristic rate scale and timescale of supply-limited transpiration under a Richards-Cowan framework. Water Resour. Res. 35 (12), 3947–3954.

Lhomme, J.P., 1997. Towards a rational definition of potential evaporation. Hydrol. Earth Sys. Sci. 1 (2), 257–264.

Luquet, D., Vidal, A., Dauzat, J., Bégué, A., Olioso, A., Clouvel, P., 2004. Using direccional TIR measurements and 3D simulations to assess the limitations and opportunities of water stress indices. Remote Sens. Environ. 90, 53–62.

Menenti, M., Choudhury, B.J., 1993. Parameterization of land surface evaporation by means of location dependent potential evaporation and surface temperature range. Exchange processes at the land surface for a range of space and time scales, Yokohama, Japan, IAHS.

Moran, M.S. 2004. Thermal infrared measurement as an indicator of planet ecosystem health. Thermal remote sensing in land surface processes. D. Quattrochi, CRC- Taylor & Francis, pp. 257–282.

Moran, M.S., Clarke, T.R., Inoue, Y., Vidal, A., 1994. Estimating crop water deficit using the relation between surface–air temperature and spectral vegetation index. Remote Sens. Environ. 49 (3), 246–263.

Olioso, A., Inoue, Y., Ortega-Farias, S., Demarty, J., Wigneron, J.-P., Braud, I., Jacob, F., Lecharpentier, P., Ottlé, C., Calvet, J.-C., Brisson, N., 2005. Future directions for advanced evapotranspiration modeling: assimilation of remote sensing data into crop simulation models and SVAT models. Irrig. Drainage Syst. 19 (3–4), 377–412.

Pellenq, J., Boulet, G., 2004. A methodology to test the pertinence of remote-sensing data assimilation into vegetation models for water and energy exchange at the land surface. Agronomie 24, 197–204.

Prihodko, L., Goward, S.N., 1997. Estimation of air temperature from remotely sensed surface observations. Remote Sens. Environ. 60 (3), 335–346.

Richards, L.A., 1931. Capillary conduction of liquids through porous media. Physics 1, 318–333.

Sandholt, I., Rasmussen, K., Andersen, J., 2002. A simple interpretation of the surface temperature/vegetation index space for assessment of surface moisture status. Remote Sens. Environ. 79 (2–3), 213–224.

Seguin, B., Itier, B., 1983. Using midday surface–temperature to estimate daily evaporation from satellite thermal IR data. Int. J. Remote Sens. 4 (2), 371–383.

Seguin, B., Becker, F., Phulpin, T., Gu, X.F., Guyot, G., Kerr, Y., King, C., Lagouarde, J.P., Ottlé, C., Stoll, M.P., Tabbagh, A., Vidal, A., 1999. IRSUTE: a minisatellite project for land surface heat flux estimation from field to regional scale. Remote Sens. Environ. 68, 357–369.

Sepulcre-Canto, G., Zarco-Tejada, P.J., Jimenez-Munoz, J.C., Sobrino, J.A., de Miguel, E., Villalobos, F.J., 2006. Detection of water stress in an olive orchard with thermal remote sensing imagery. Agric. Forest Meteorol. 136 (1–2), 31–44.

Shuttleworth, W.J., Wallace, J.S., 1985. Evaporation from sparse crops—an energy combination theory. Q. J. R. Meteorol. Soc. 111, 839–855.

Su, Z., 2002. The surface energy balance (SEBS) for estimation of turbulent fluxes. Hydrol. Earth Sys. Sci. 6 (1), 85–99.

Suleiman, A., Crago, R., 2002. Analytical land–atmosphere radiometer Model. J. Appl. Meteorol. 41, 177–187.

Vidal, A., Devaux-Ros, C., 1995. Evaluating forest fire hazards with Landsat TM derived water stress index. Agric. Forest Meteorol. 77, 207–224.

Yuan, G., Luo, Y., Sun, X., Tang, D., 2004. Evaluation of a crop water stress index for detecting water stress in winter wheat in the North China Plain. Agric. Water Manage. 64 (1), 29–40.